# Seismicity and active accretion processes at the ultraslow-spreading Southwest and intermediate-spreading Southeast Indian ridges from hydroacoustic data

Eve Tsang-Hin-Sun, Jean-Yves Royer, Julie Perrot

Geophysical Journal International

*Geophys. J. Int.* (2016) **206,** 1232–1245
Advance Access publication 2016 May 29
GJI Marine geosciences and applied geophysics

doi: 10.1093/gji/ggw201

# Seismicity and active accretion processes at the ultraslow-spreading Southwest and intermediate-spreading Southeast Indian ridges from hydroacoustic data

Eve Tsang-Hin-Sun,[1,2] Jean-Yves Royer[1,2] and Julie Perrot[1,2]

[1] *University of Brest, Laboratoire Domaines Océaniques, Brest, France. E-mail: jean-yves.royer@univ-brest.fr*
[2] *CNRS, Laboratoire Domaines Océaniques, Brest, France*

Accepted 2016 May 25. Received 2016 May 24; in original form 2015 November 27

## SUMMARY

Volcanic and tectonic events are the main processes involved in the generation of the oceanic crust and responsible for the seismicity associated with seafloor spreading. To monitor this activity, usually not or poorly detected by land-based seismological stations, we deployed from February 2012 to February 2013 a network of autonomous hydrophones to compare the behaviour of the ultraslow-spreading Southwest Indian ridge (SWIR) with that of the intermediate-spreading Southeast Indian ridge (SEIR). The rate of seismicity is similar for both ridges, suggesting that there is no systematic relationship between seismicity and spreading rates. The along-axis distribution of the seismic events, however, does differ, reflecting the rate dependence of accretion modes. Earthquakes are sparse and regularly spaced and scattered along the SWIR, reflecting prevailing tectonic processes. By contrast, along the SEIR, events are irregularly distributed and focus at ridge-segment ends and transforms faults, reflecting the ridge segmentation; only two swarms occurred at a segment centre and are probably caused by a magmatic event. This seismicity distribution thus looks controlled by segment-scale crustal heterogeneities along the SEIR and by regional-scale contrasting accretion processes along the SWIR, probably driven by different lithospheric and asthenospheric dynamics on either side of the Melville fracture zone. The comparison of hydroacoustic and teleseismic catalogues shows that, along these spreading ridges, the background seismicity observed in 1 yr by a hydroacoustic network is representative of the seismicity observed over two decades by land-based networks.

**Key words:** Seismicity and tectonics; Acoustic properties; Mid-ocean ridge processes; Indian Ocean.

## 1 INTRODUCTION

Volcanic and tectonic events are the fundamental processes involved in the generation of the oceanic crust and responsible for the seismicity associated with seafloor spreading. Yet, these episodes are usually not or poorly recorded by land-based seismological networks due to the rapid attenuation of seismic waves in the solid Earth. However, because mid-oceanic earthquakes produce a low-frequency hydroacoustic phase (T-phase) that propagates in the water column over long distances with little attenuation (e.g. Fox & Squire 1994), arrays of autonomous hydrophones (AUHs) are able to capture the low-level seismicity associated with seafloor spreading processes along mid-oceanic ridges (MORs).

Hydroacoustic experiments, conducted in the Northeast and East Pacific and in the Atlantic oceans, have revealed the distribution of the low-level seismicity along the ultrafast to fast-spreading East Pacific Rise (EPR; Fox *et al*. 2001), the intermediate-spreading Juan de Fuca and Gorda ridge systems (Dziak *et al*. 1995; Fox & Dziak 1998; Bohnenstiehl *et al*. 2004; Dziak *et al*. 2011) and the slow-spreading Mid-Atlantic Ridge (MAR; Smith *et al*. 2002; Simão *et al*. 2010; Goslin *et al*. 2012). Excluding the seismic activity of transform faults, fast-spreading ridge segments, such as the EPR, generally have a low seismicity rate whereas slow-spreading ridge segments, such as the MAR, produce a high level of seismicity probably related to a colder thermal regime. Between these end-members, intermediate-spreading ridges present both types of seismicity, depending on their morphology (Bohnenstiehl & Dziak 2008; Dziak *et al*. 2012). In the Northeast Pacific, for instance, the Gorda Ridge exhibits a constant along-axis seismic activity, while the Juan de Fuca Ridge has nearly aseismic segments (Dziak *et al*. 2012), although both ridges have a similar spreading rate (60 mm $y^{-1}$ full rate). However, these studies mainly focused on ridges with spreading rates larger than 25 mm $y^{-1}$. At ultraslow spreading rates, the nature of the accretion processes undergoes

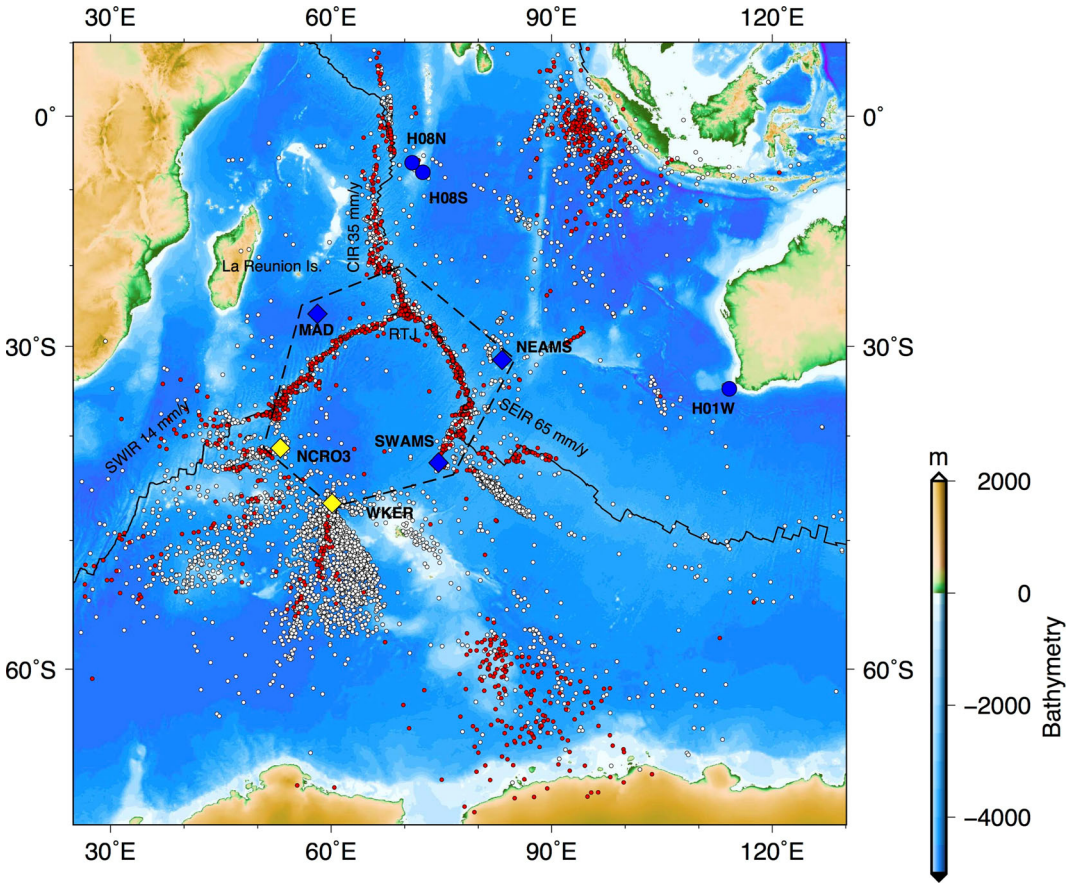


**Figure 1.** Location of hydroacoustic events recorded in 2012 by the OHASISBIO network of hydrophones (yellow and blue diamonds). Events located by four or more hydrophones are in red, otherwise in white. The dashed polygon outlines the study area of study, where location uncertainties are generally better than 5 km. Blue diamonds indicate the three hydrophones used in the DEFLO experiment in 2007 (MAD, SWAMS and NEAMS). Blue circles are the permanent hydroacoustic stations of the International Monitoring System (IMS) in the Indian Ocean.

fundamental changes as the colder thermal regime of the lithosphere reduces the melt supply in the axial lithosphere (Reid & Jackson 1981; Cannat *et al*. 1995; Dick *et al*. 2003). Moreover, comparative studies rely on seismological data sets with different completeness levels and might thus not reflect entirely the variation in seismicity rate with spreading rate.

Magmatism is one of the two processes generating earthquakes in the oceanic crust. Events of magmatic origin include any magmatic processes such as a dike emplacement or propagation at depth, a replenishment of a magma chamber, hydrothermal circulation or an eruption of lava on the seafloor. These events are relatively frequent at fast to intermediate spreading rates, producing swarms of hundreds of events (e.g. Dziak *et al*. 2007). At slow-spreading rates, earthquake swarms are larger but less frequent. One of the largest observed magmatic swarms occurred along the ultraslow Gakkel Ridge (6–12 mm $y^{-1}$ full rate; Tolstoy *et al*. 2001; Schlindwein 2012), suggesting that there is a first-order relationship between the size and frequency of magmatic swarms and the spreading rate. The Indian Ocean is a unique place to investigate the relationship between seismicity and spreading rates due to the presence of three MORs with contrasting rates (Fig. 1), which can be simultaneously monitored with a single hydrophone network providing homogeneous data sets for each ridge. Any differences in the data acquisition (hydrophone specifications, duration of experiment, etc.) and data processing often hinder the comparison of catalogues from different hydrophone arrays.

The ultraslow spreading Southwest Indian Ridge (SWIR) is one of the slowest ridges in the world, spreading at 14 mm $y^{-1}$ full-rate, and represents a low end-member in terms of magma supply (Cannat *et al.* 1999, 2008). The easternmost part of the ridge, between the Rodrigues Triple Junction (RTJ) and the Melville fracture zone (FZ at 61°E), is also one of the deepest spreading systems (Mendel *et al*. 1997; Cannat *et al*. 1999). East of the Melville FZ, the ridge segmentation and morphology differ drastically from what is observed westwards and from faster spreading ridges. Two particularities of ultraslow-spreading ridges are the apparent absence of volcanic activity over large areas of the seafloor where mantle-derived peridotites are instead exposed (Dick *et al*. 2003; Sauter *et al*. 2004; Cannat *et al*. 2006) and the presence of large detachment faults that, through tectonic extension, accommodates a high amount of the plate separation (Sauter *et al*. 2013). At the same time in these areas, the volcanic crust is found to be anomalously thin (Minshull & White 1996; Minshull *et al*. 2006).

The slow-spreading Central Indian Ridge (35 mm $y^{-1}$) and the intermediate-spreading Southeast Indian Ridge (SEIR, 60 mm $y^{-1}$) are the two other branches of the Indian Ocean spreading system. Intermediate-spreading ridges represent the critical state at which a continuous melt lens might exist along the axis (Small & Sandwell 1989; Morgan & Chen 1993). Thus, small changes in the thermal structure can have large consequences on the nature of the seismic processes of the ridge. Geophysical data along the westernmost part of the SEIR, from the RTJ to the St-Paul and Amsterdam Plateau

have shown that seafloor spreading results from a succession of volcanic and tectonic processes (Sauter *et al*. 1991), with more abundant magmatism in the vicinity of the St-Paul and Amsterdam hot-spot (Johnson *et al*. 2000; Scheirer *et al*. 2000; Maia *et al*. 2011). Most seismicity studies along the Indian MOR are based on teleseismic data (Sykes 1970; Bergman *et al*. 1984; Schlindwein 2012) and thus on moderate- to large-sized earthquakes ($M > 4$–5). Hanson & Bowman (2005), Yun *et al*. (2009) and Royer *et al*. (2015) presented the first analyses of the small magnitude seismicity, based on hydroacoustic records.

With such spreading ridge configuration, the Indian Ocean is a unique place to study the relationships between spreading and seismicity rates and their along-axis variations, with a single array. To this effect, from February 2012 to February 2013, a network of seven AUHs has been deployed to record the low-level seismicity associated with the SWIR and SEIR. This paper describes the observed patterns in the seismicity along these ridges, discusses the spatio-temporal distribution of the seismic activity and its variations at different scales and examines the relationship between spreading and seismicity rates.

## 2 HYDROACOUSTIC DATA AND METHOD

As a follow-up to the DEFLO test-experiment in 2007 (Royer *et al*. 2015), the OHASISBIO project aims at monitoring the seismicity of the three Indian MORs as well as the biodiversity through the recording of blue whales calls in the Southern Indian Ocean (e.g. Samaran *et al*. 2013). Taking advantage of the annual voyages of the RV *Marion Dufresne* to the French islands in the Southern Indian Ocean, the OHASISBIO network comprises seven AUHs located at five widely distributed sites and simultaneously and continuously monitoring an area of about 3000 × 4800 km$^2$ (Fig. 1). The instruments are moored in the axis of the Sound Fixing And Ranging channel, 500–1300 m below the sea surface depending on the location. This paper reports on the data collected during the third deployment of the network, from February and March 2012 to January and February 2013. The instruments consist of a hydrophone connected to an acquisition and storage system developed by the Laboratoire Domaines Oceaniques (Brest, France; D'Eu *et al*. 2012). The acoustic data are digitized at a sampling rate of 240 Hz using a 24-bit analogue-to-digital conversion. Each instrument is synchronized, at deployment and recovery, with the GPS time; clock-drifts range from 1 to 5 s, which over the deployment duration represent a drift of few $10^{-8}$ s s$^{-1}$. Raw data are thus corrected for the measured clock-drift and for the instrument sensitivity and gain provided by the manufacturer.

The data were processed as described in Royer *et al*. (2015). The seismic events were detected and located with the 'Seas' analysis software developed by the Pacific Marine Environment Laboratory (Fox *et al*. 2001). The acoustic magnitude or Source Level (SL) of the events, expressed in decibels with respect to 1 micro-Pascal at 1 meter (dB re μPa at 1 m), was recomputed independently, as the median of the received acoustic levels at each hydrophone corrected for the transmission loss over the distance from the hydrophone to the epicentre. The received acoustic level (RL) is the root mean square of the signal amplitudes over a window of 10 s centred on the picked arrival time (i.e. maximum energy arrival). The $RL_{rms}$ is about 15 dB less than the RL peak-to-peak used by Royer *et al*. (2015). The latter is closer to the seismological definition of magnitude, whereas the former is probably more representative of the acoustic energy radiated by the seismo-acoustic conversion zone.

**Table 1.** Comparison between the DEFLO and OHASISBIO hydroacoustic catalogues. Source level completeness (SLc) based on Fig. 4.

| | DEFLO (2007) | OHASISBIO (2012) |
|---|---|---|
| Number of events[a] | 4526 (10105) | 5133 (8067) |
| Number of events inside the polygon[a,b] | 767 (1253) | 1750 (2883) |
| Source Level of completeness ($SL_c$ in dB) | 205 | 215 |
| Number of events with SL > $SL_c$ | 447 | 1013 |

[a]Detected by 4 AUH or more (and total number).
[b]Polygon shown in Fig. 1.

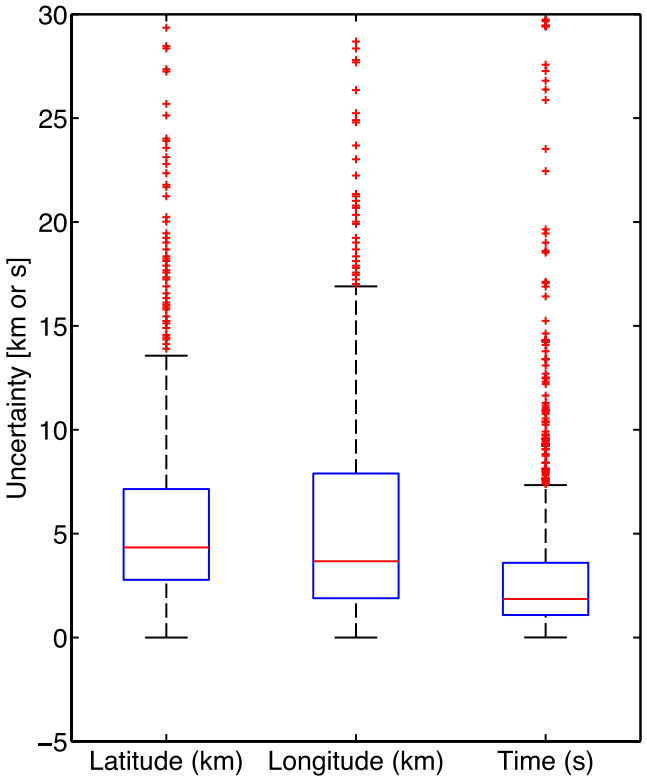


**Figure 2.** Boxplot distribution of the location and origin-time uncertainties ($2\sigma$) for the hydroacoustic events inside the polygon of Fig. 1. The blue box contains 50 per cent of the distribution and the red line, inside the box, shows the median value of the distribution (less than 5 km in latitude and longitude, and 2 s in origin time). Dashed lines represent the range of uncertainties (minimum and maximum) and red crosses, outliers of the distribution.

In the period of observation, nearly 8000 events were detected, of which ∼2900 occurred inside the array and ∼5100 outside (Fig. 1, Table 1). Among the latter, most of them are located south of 40°S and correspond to ice-tremors and ice-quakes originating from the southern latitudes, as observed in other acoustic catalogues (Chapp *et al*. 2005; Hanson & Bowman 2005; Royer *et al*. 2015). Outside the hydrophone network, location uncertainties are large or unknown when based on only three instruments (white symbols in Fig. 1); apparent alignments are artefacts due to the array geometry and/or to the blocking or deflecting effects of submarine reliefs to acoustic waves. Inside the network (polygon in Fig. 1), the median uncertainties are 2 s in origin time and smaller than 5 km in longitude or latitude at the 95 per cent confidence level (Fig. 2). Hereinafter, only the 1750 events recorded by at least four hydrophones are considered. In the same polygon and during the

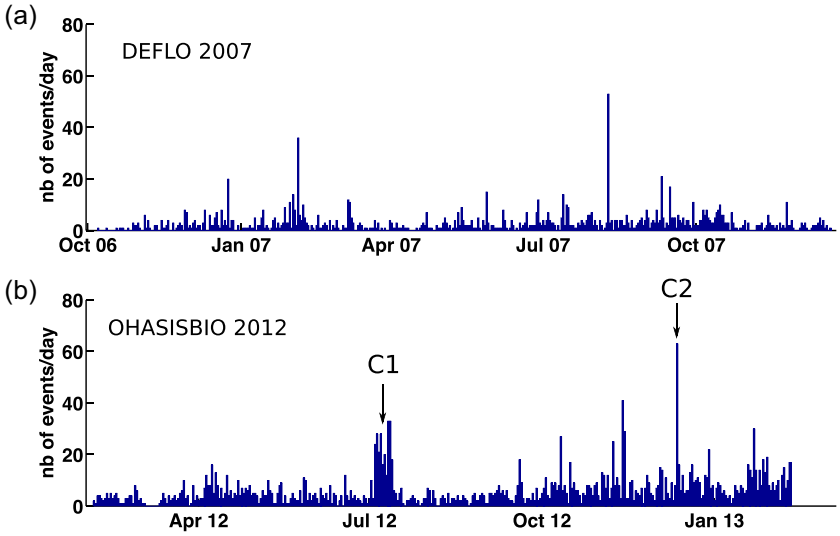


**Figure 3.** Number of events located with the DEFLO (top) and OHASISBIO (bottom) hydrophone networks, within the polygon defined in Fig. 1. High and narrow peaks of seismicity are clusters of events. The DEFLO experiment detected less events than the OHASISBIO experiment, which is consistent with the respective size and number of hydrophones of each network.

same recording period, the National Earthquake Information Centre reported only 53 events and the International Seismological Centre bulletin 181 events (ISC 2013). On average, the OHASISBIO array detected about twice more events than the DEFLO array (Table 1) probably due to a better geometry and coverage of the hydrophone array towards the Java trench relative to the initial experiment that comprised only three AUHs supplemented by the two distant International Monitoring System (IMS) permanent stations in Diego Garcia and Cape Leeuwin (Fig. 3). The two peaks in the number of events, in July and December 2012, correspond to two large clusters of events.

The detection threshold of the array or Source Level of completeness ($SL_c$) of the OHASISBIO catalogue can be derived from the frequency-size distribution of the acoustic events. Our analysis is based solely on the 1750 events located inside the array. The $SL_c$ is defined in an analogue manner as the magnitude of completeness (Bohnenstiehl *et al*. 2002) and is estimated by fitting a Gutenberg–Richter relationship to the catalogue of events (Gutenberg & Richter 1944):

$$\log(N) = a - b\,\mathrm{SL}, \tag{1}$$

where $N$ is the number of events having a Source Level greater or equal to SL and $a$ and $b$ are constants determined with the maximum likelihood method (Aki 1965). The OHASISBIO catalogue displays an $SL_c$ of 215 dB higher than the DEFLO $SL_c$ of 205 dB (Fig. 4; Table 1). The roll-off point of the relationship corresponds to 1050 events $yr^{-1}$ for OHASISBIO and 640 for DEFLO suggesting that the OHASISBIO array is more sensitive than the DEFLO array despite a higher $SL_c$. Moreover, both distributions have the same $b$-value and display a systematic difference in the Source Levels, which could be explained by an error of 10 dB in the sensitivity of the hydrophones used for these two experiments, rather than different limits of detection. Inter-calibrating hydrophones would require mooring two of each kind at the same site. In this study, only events with a Source Level equal or above the estimated $SL_c$ are considered for computing the seismicity rate. A magnitude of completeness of $m_b = 3.3$ can be estimated by extrapolating the frequency-size distribution of the teleseismic events up to the number of events defining the AUH $SL_c$ (Fig. 4). That is to say that the hydrophone network detected in 1 yr about five times more events than the teleseismic network.

To examine the time-clustering behaviour of the seismicity along the spreading ridges, we run a cluster analysis over the catalogue, using the Single Link Cluster method of Frohlich & Davis (1990), based on a space–time metric $D$ describing the proximity of two events by

$$D = \sqrt{d^2 + t^2}, \tag{2}$$

where $d$ is the distance (km) and $t$ the time interval (days) between two events. Clusters are then defined as events within a $D_c$ radius set as $D_c = 0.8D_1$, where $D_1$ is the median length of all $D$ within the catalogue (Nyffenegger & Frohlich 2000). The choice of this method is based on its successful application to other hydroacoustic catalogues (e.g. Bohnenstiehl *et al*. 2002; Simão *et al*. 2010). The analysis of our 2012 catalogue only detected five clusters of 20 events or more, along the SEIR (4) and the SWIR (1). These clusters are removed from the catalogue to compute unbiased seismicity rates along each MOR, here defined as the number of events in bins of 20 km along the ridge axis. In this paper, all along-axis distances are calculated from the RTJ relative to the Somalia/Antarctica and Capricorn/Antarctica rotation poles of DeMets *et al*. (2010), for the SWIR and the SEIR, respectively (events along a transform fault will thus be at the same distance from these opening poles). The ISC bulletin is analysed for the period 1995–2012 in the same way as the acoustic catalogues.

## 3 SEISMICITY OF THE SOUTHWEST INDIAN RIDGE

The seismicity along the SWIR, from the RTJ (70°E) to the Gallieni FZ (52°E), displays different patterns (Figs 5 and 6). In the vicinity of the triple junction, events tend to cluster along the reliefs bordering the axial valley. Between 69°E and the Melville FZ, events are sparse but regularly spaced and scattered up to 50 km off-axis. The seismicity is mainly located south of the ridge axis, along abyssal hills parallel to the axis (Fig. 7). West of the Melville FZ, this asymmetry is less pronounced and events are closer to the axial region. Groups of events also focus at the intersections of spreading-ridge

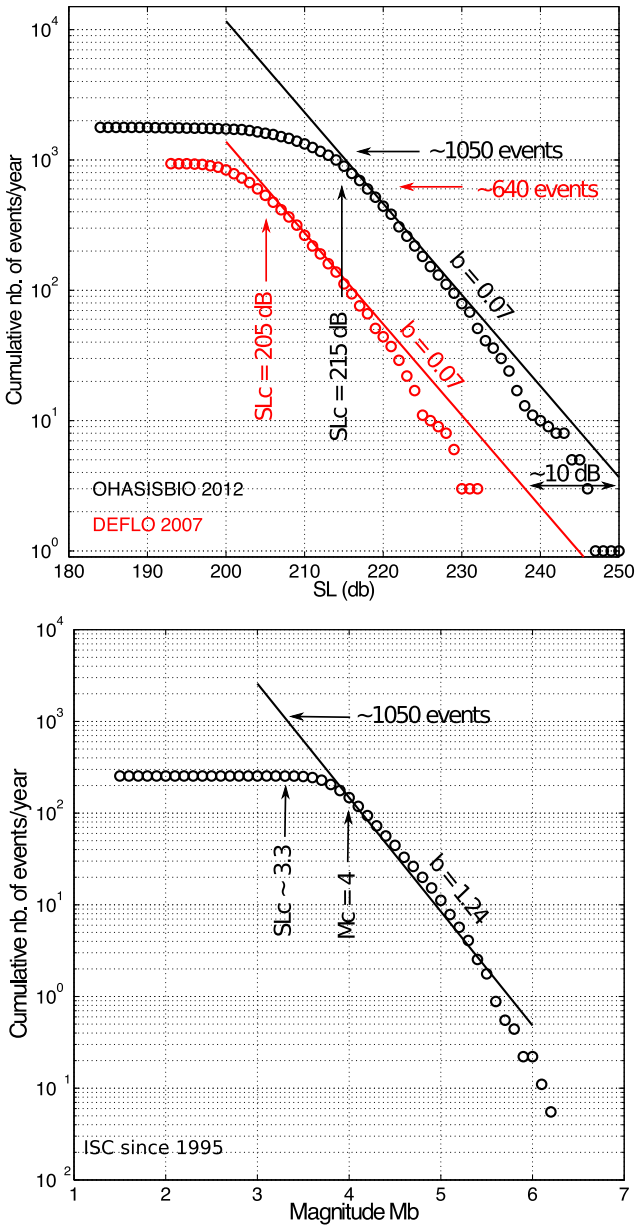


**Figure 4.** Size–frequency distributions for the DEFLO and OHASISBIO catalogues (top) and for the ISC teleseismic catalogue (bottom). Extrapolating the Gutenberg–Richter relationship of the ISC data up to the number of events for which the acoustic catalogues are complete yields a level of completeness of $m_b \sim 3.3$ for OHASISBIO and $m_b \sim 3.5$ for DEFLO.

segments with transform faults (Novara TF, Atlantis II TF, Gazelle TF) and at some ridge segments, but are not time-clustered.

Overall, the rate of seismicity along the SWIR is low, with less than 10 events per 20 km in 2012 (Fig. 6). The seismicity rate is higher (up to 10 events/20 km) between the triple junction and 69°E (∼100 km west of the RTJ) than west of 69°E to the Melville FZ where it falls to 5 events per 20 km or less. The number of events increases again west of Melville FZ (up to 20 events/20 km between Gauss and Gazelle TF, ∼7 events/20 km elsewhere). Similar seismicity rates are observed in the 2007 hydroacoustic catalogue and in the 1995–2015 land-based seismic catalogue (ISC; Fig. 6), with a very low event rate between 69°E and the Melville FZ and a slight increase west of Melville FZ where the Atlantis II and Gallieni TF are the most active areas. The ISC catalogue displays a peak of events at 65.5°E (420 km from the RTJ), due to a large swarm of magmatic origin that occurred in 1997 and 1998 (Schlindwein 2012). In the 2007 and 2012 catalogues, hydroacoustic events rarely occur in clusters and are generally sparse in space and time. Only two seismic clusters occurred in January 2007 at the inside corner of the Atlantis II TF (26 events) and in October 2012 near the Gazelle TF (29 events; Fig. 6). In both cases, the time distribution of these clusters, comparable to an Omori's law, suggests seismic sequences of shock and aftershocks, although the small number of events and large location-uncertainties make them difficult to analyse. Thus, both the long-term (20 yr) medium-level "land-based" seismicity and the yearly (2007 and 2012) low-level hydroacoustic seismicity along the SWIR are characterized by a low background activity with isolated and punctual clusters (only one teleseismic cluster over two decades and two hydroacoustic clusters over 2 yr) from the RTJ to the Gallieni FZ.

Large earthquakes ($M_w \geq 5$) from 1995 to 2012 are common although irregularly distributed along the SWIR axis (Fig. 6). East of Melville FZ, they are associated with a large magmatic swarm at 65.5°E and with a short (100 km) segment adjacent to the Melville FZ. West of Melville FZ, large magnitude events are more abundant and scattered along the segments. Although Source Levels do not directly represent seismic magnitudes, a similar pattern is observed in the hydroacoustic data and high-SL events are more abundant west than east of the Melville FZ. East of Melville FZ, these high-SL events occur on the same segments as the large magnitude teleseismic events.

In terms of large-scale along-ridge variations, three supersegments, bounded by major transform offsets, can be defined: between the RTJ and the Melville FZ (RTJ_MEL), from the Melville to Atlantis II FZ (MEL_ATL) and from the Atlantis II to Gallieni FZ (ATL_GAL). To ease their comparison, the number of events is normalized to a distance of 100 km in each supersegment and for each hydroacoustic (2007, 2012) and land-based (since 1995) catalogues (Table 2). In 2007 and 2012, the pattern of seismicity is very similar. The RTJ_MEL supersegment has the lowest level of seismicity while the two other supersegments have a similar and more important activity. The events in the ISC bulletin for the last two decades shows the same seismic patterns; the RTJ_MEL supersegment is less active than the MEL_ATL and ATL_GAL, which exhibit similar activity rates. The Melville FZ thus acts as a boundary between contrasted seismic regions and this observation seems persistent over annual and decadal timescales. Table 2 also shows that the level of activity detected by land-based networks over 9 yr (1995–2004 and 2004–2012) is similar to the yearly levels measured by acoustic arrays.

## 4 SEISMICITY OF THE SOUTHEAST INDIAN RIDGE

The seismicity along the SEIR is less scattered than along the SWIR and tends to cluster in specific areas (Fig. 8). Except at the southern extremity of the SEIR, where large longitude-uncertainties tend to bias the epicentre locations, events are located close to the ridge axis (within 10–20 km) but mainly occur at segment ends and along transform faults. The only exception is the ridge segment at 29°S, which exhibits at its centre clear time-clusters. The most active transform faults are located on the St-Paul and Amsterdam Plateau (Amsterdam TF, Boomerang TF, Hilegom TF) where the highest Source Levels are also recorded. In general, SLs are also higher

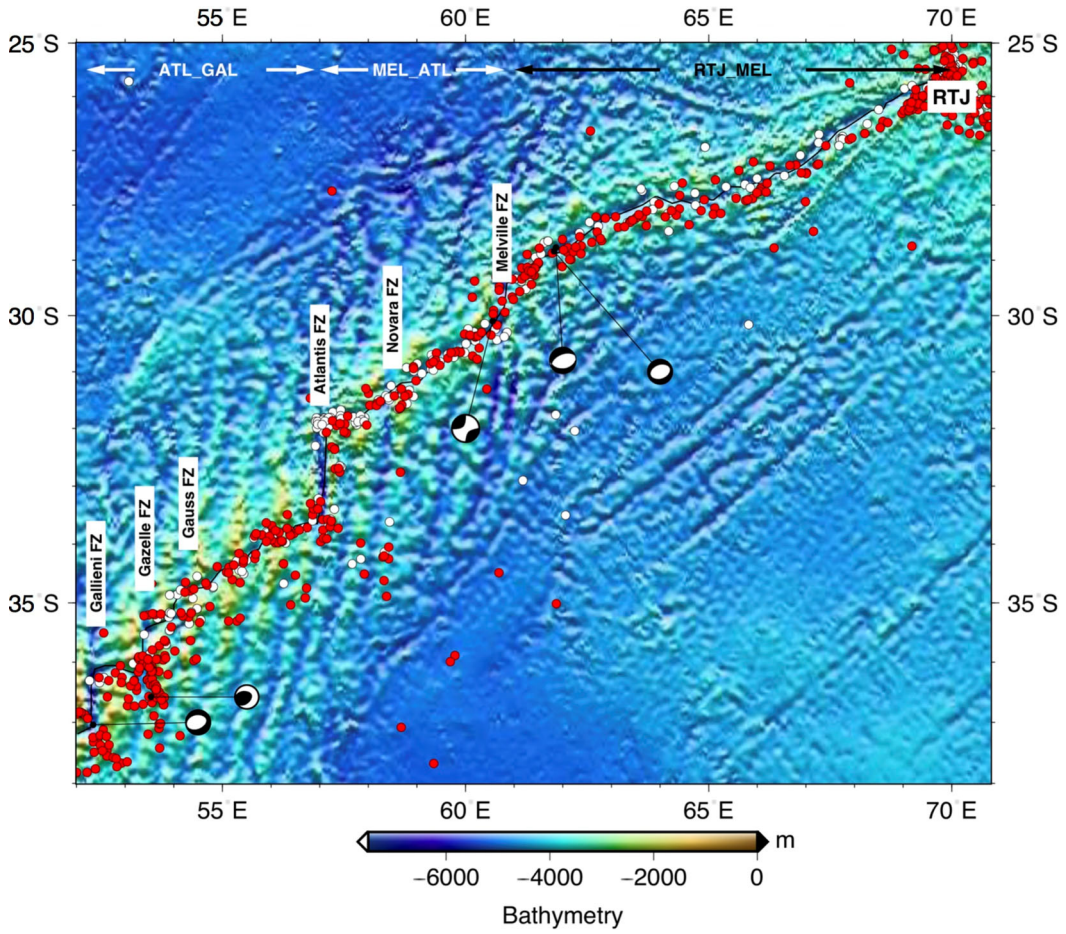


**Figure 5.** Location of the events recorded by the OHASISBIO array in 2012 (red) and by the DEFLO array in 2007 (white), along the Southwest Indian Ridge. Only events located by 4 AUH or more are shown; location uncertainties are smaller than the symbol size. The three supersegments (top), bounded by major transform faults, display different seismicity patterns (see text and Table 2). Only five moment tensor solutions were determined in 2012 (Global Centroid Moment Tensor database, Ekström *et al*. 2012). The black line represents the SWIR axis. Gridded bathymetry from Mendel *et al*. (1997).

along transform faults than in segment centres. The seismicity along transform faults appears to be continuous in time or clusters in short duration sequences (Fig. 9). The centres of ridge segments generally appear as seismic gaps at the $m_b = 3.3$ level of completeness, except for one segment at 29°S. Thus the seismicity rate varies irregularly along the ridge axis, being low in segment centres and high at segment ends and along transform offsets. The event rate is 1 to 10 events per 20 km and increases up to ∼20 events per 20 km near the St-Paul and Amsterdam Plateau. The patchy seismicity of the SEIR thus differs from the evenly distributed seismicity along the SWIR.

The same observation stands for the 2007 hydroacoustic and 1995–2005 ISC catalogues (Fig. 9). The most active faults are the same, illustrating the persistence of their activity and associated seismicity. The ridge segments at 27°S and 29°S are the most active, presenting a nearly continuous activity since 1995. Two small clusters, in 2002 and 2005 (8 and 9 events, respectively), are found in the vicinity of an inactive hydrothermal site at about 28°S, 74°E (Fig. 8; Beaulieu 2010). The SEIR intersection with the St-Paul and Amsterdam Plateau is consistently the most seismically active area and transform faults produce large and recurrent earthquakes ($M_w \geq 5$; Fig. 8). Throughout the SEIR, events at segment centres and transform faults are otherwise scarce, isolated and with lower magnitudes. This general good agreement between land-based and hydroacoustic catalogues suggests, as for the SWIR, that the pattern of seismicity observed in 1 yr by a hydroacoustic network is representative of the seismicity observed over two decades by land-based networks.

Four clusters are identified along the SEIR, using the SLC method (Frohlich & Davis 1990). Two of them are located on the St-Paul and Amsterdam Plateau and two others, C1 and C2, the largest, are located at the centre of a ridge segment at about 29°S, 620 km away from the triple junction (Figs 9–11). The first cluster C1 initiated in June 2012 and comprises 184 events over 46 d (Fig. 10). The majority of events, however, occurred between the 8th and 10th day after the first event. The second cluster, C2, is located just few kilometres north (Fig. 11) and occurred 6 months after C1. It is composed of 64 events that lasted for 3 weeks, with a peak of events during the first day (Fig. 10). Both clusters present similarities: the absence of a dominant main shock initiating the sequence, a high number of events with respect to time, and a relative homogeneity in the Source Levels within each cluster. These characteristics, common to other swarms at spreading centres (e.g. Dziak *et al*. 1995; Dziak & Fox 1999), have been associated to a magmatic activity by analogy to sub-aerial volcanoes (e.g. Einarsson & Brandsdottir 1980). Few events are also reported in the ISC bulletin, with magnitudes ($m_b$) rarely exceeding 4. Only two events, on July 12, at the end of the main period of activity, have a moment magnitude ($M_w = 4.9$ and 5.0) and normal faulting mechanisms (Figs 10 and 11); they match acoustic events with a SL of 214 and 218 dB, respectively. These events probably reflect a strain adjustment on existing faults.

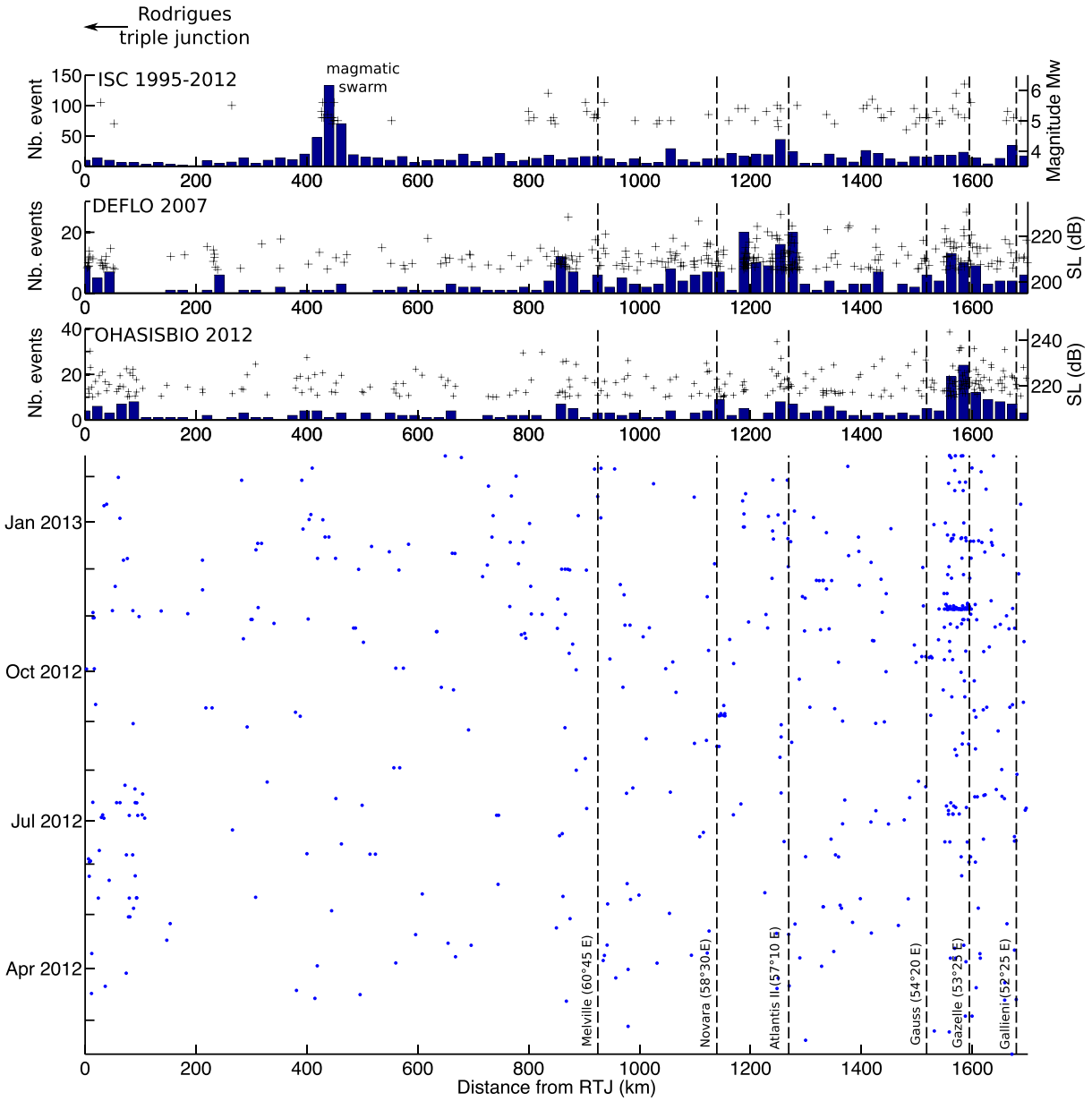


**Figure 6.** Spatial and temporal distribution of the seismicity along the Southwest Indian Ridge. Histograms (top) show the number of events in bins of 20 km for the teleseismic ISC catalogue, and the hydroacoustic DEFLO and OHASISBIO catalogues. In the ISC histogram, black crosses indicate the moment magnitude of strong earthquakes. In the DEFLO and OHASISBIO histograms, black crosses indicate the Source Level or acoustic magnitude of events with $SL \geq SL_c$. In the time–distance distribution of the events (bottom), transform faults are plotted as dashed lines.

In favour of a magmatic origin for cluster C1, events with location uncertainties smaller than 5 km evidence a clear migration of the epicentres to the south along the axis, with a migration rate of 0.05 m $s^{-1}$ during 10 d (Fig. 12). After 2012 July 8, however, events scatter over the whole ridge segment. No clear migration pattern is observed in cluster C2, where the peak of activity occurred in less than a day.

## 5 DISCUSSION

### 5.1 Seismicity rate

There is a first-order contrast in the seismicity rate of MORs as a function of spreading rate (Bohnenstiehl & Dziak 2008). Fast-spreading ridges generally produce a low level of seismic activity while slow spreading ridges display a larger amount of earthquakes. At intermediate spreading rates, the seismicity can match both patterns, showing that the seismicity rate is not linked only to the spreading rate. We find, however, that the Southwest and Southeast Indian spreading centres both exhibit the same low levels of background seismicity, for a $m_b = 3.3$ level of completeness. Excluding FZs from the event distribution, the median rate is 4 events per 20 km for both ridges, while the mean rate is 4 events per 20 km for the SWIR and 6 events per 20 km for the SEIR. Even though the SEIR spreads four times faster than the SWIR, the difference in seismicity rate is not significant, at the considered level of completeness. In 2007, the median seismicity rate is 1 event and 3 events per 20 km for the SEIR and SWIR, respectively.

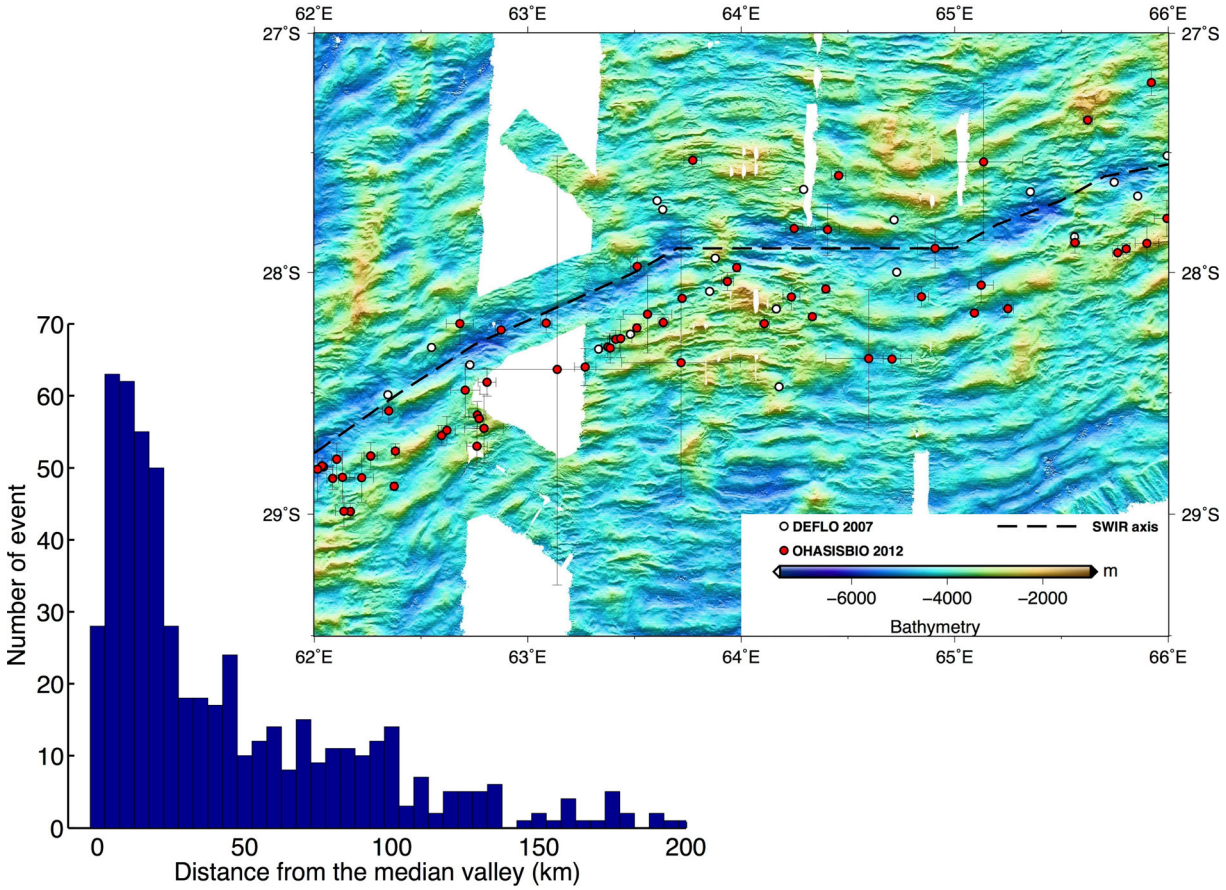


**Figure 7.** Distribution of the orthogonal distances of the epicentres relative to the SWIR axis and close-up of Fig. 5 between 62°E and 66°E; error bars show the ($2\sigma$) location uncertainties. Red and white symbols represent the 2012 and 2007 catalogues, respectively. Detailed gridded bathymetry from Cannat *et al.* (2006).

**Table 2.** Number of declustered events normalized to a length of 100 km in each of the supersegments along the Southwest Indian Ridge shown in Fig. 5. The total number of events in each supersegment is given in brackets for the two hydroacoustic catalogues.

| Supersegment | Length (km)[a] | DEFLO events/ 100 km | OHASISBIO events/ 100 km | ISC events/ 100 km[b] |
|---|---|---|---|---|
| RTJ to Melville FZ | 925 | 18 [169] | 15 [134] | 22 (29) |
| Melville to Atlantis FZs | 345 | 31 [108] | 22 [77] | 37 (35) |
| Atlantis to Gallieni FZs | 410 | 32 [130] | 37 [151] | 34 (27) |

[a]Projected onto great circles passing through the Somalia/Antarctica pole of rotation (see the text).
[b]For equal time periods of 9 yr: 2004–2012 and 1995–2003 in parentheses.

In terms of seismicity level, the SEIR is very similar to the Juan de Fuca Ridge, which appears mostly aseismic at a similar level of completeness (Dziak *et al*. 2011). The SWIR does not show a striking contrast to these intermediate-spreading ridges, although its spreading rate is much lower and tectonic processes are predicted to accommodate a higher amount of the deformation (Sauter *et al*. 2013). This may imply that seafloor spreading occurs either aseismically or with very low-level magnitude seismicity, not recorded by the AUH. The presence of serpentinized peridotites over large sections of the SWIR (Dick *et al*. 2003; Cannat *et al*. 2006, 2008) possibly weakens the strength of the lithosphere (Escartin *et al.* 1997, 2001; Hirth & Guillot 2013) and could contribute to a largely aseismic behaviour of the brittle layer. Nonetheless, observation from a local seismological network off the Gakkel Ridge suggests that amagmatic segments are seismically active, with low magnitudes ($m_b < 4$; Morozov *et al*. 2016). The similar number of events per unit of ridge-segment length along the ultraslow-spreading SWIR (1–4/20 km) and the intermediate-spreading SEIR (3–4/20 km) suggests that there is no direct relationship between spreading rates and seismicity rates.

### 5.2 Along-axis variations

The SWIR and the SEIR do differ, however, in their spatial patterns of seismicity. Along the SWIR, events are less frequent on transform faults relative to ridge segments and the earthquakes are sparse and scattered but regularly distributed along the ridge axis. East of the Melville FZ, where no transform faults offset the axis, events are even more scattered up to 100 km off the median valley (inset of Fig. 7). Events generally align along abyssal hills, parallel to the ridge axis, especially in the oblique-spreading section of the ridge, where tectonic extension is accommodated by normal and large

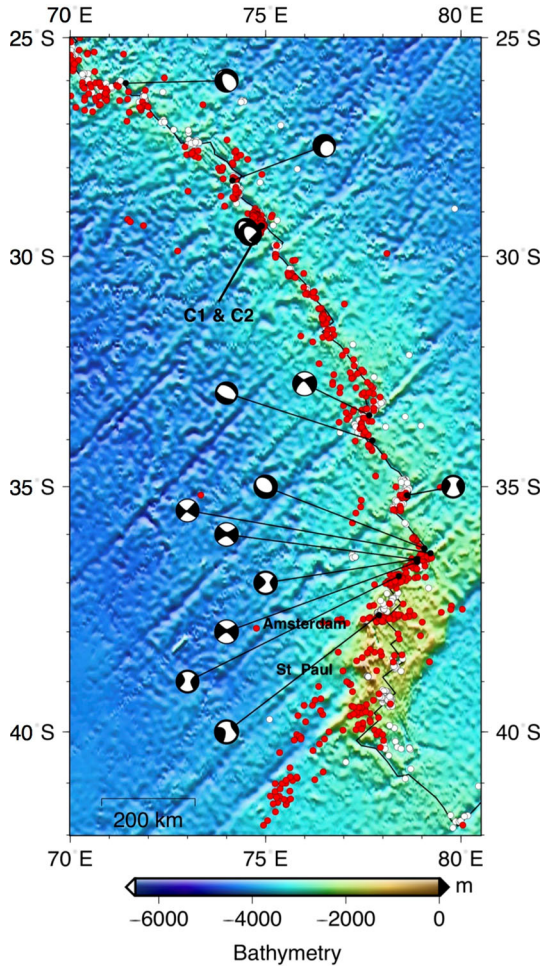


**Figure 8.** Hydroacoustic events detected by four or more hydrophones from the DEFLO array in 2007 (white circles) and the OHASISBIO array in 2012 (red circles) along the Southeast Indian Ridge (axis in black), from the Rodrigues triple junction to the St-Paul and Amsterdam Plateau. Only 14 moment tensor solutions were determined in 2012 (GCMT database). Events generally cluster at segment ends and transform faults. South of 37°S, alignments are artefacts due to the geometry of the hydrophone network and to the blocking effect of the St Paul and Amsterdam Plateau; they include events with large location uncertainties. The left-lateral strike-slip focal mechanisms in this region suggest that the events are more likely located along transform faults. Bathymetry from the ETOPO1 grid.

off-axis detachments faults (Sauter *et al*. 2013). Although such off-axis pattern is also observed at a local scale from OBS data in the vicinity of the RTJ (Katsumata *et al*. 2001) and despite the small location uncertainties for these events (Fig. 2), these off-axis alignments may be caused by the geometry of the array, since there is only one site north of the SWIR (MAD, Fig. 1). It may also be argued that this observation is an artefact of the hydroacoustic approach, which locates the acoustic source or radiator where seismic waves convert into acoustic waves and not the actual epicentre. The SWIR would be more prone to such bias due to its deep axial valley and steep flanks. A detailed comparison with microseismicity from OBS data, for instance, and a better understanding of T-wave conversion processes would help reduce this uncertainty.

In contrast, along the SEIR, segment ends and transform faults produce more and larger earthquakes than ridge-segment centres, except for one segment at 29°S, where two magmatic swarms occurred. This uneven distribution of seismicity thus suggests segment-scale variations in the lithosphere structure, as typically observed along the slow-spreading MAR (Smith *et al*. 2002; Goslin *et al*. 2012) and consistent with geological observations and models (e.g. Kuo & Forsyth 1988; Tucholke & Lin 1994). The influence of the St-Paul and Amsterdam hot-spot on this distribution is not as clear as in the vicinity of the Azores hotspot, where the seismic rate decreases towards the hot-spot as the axial lithosphere becomes hotter and thinner (Goslin *et al*. 2012). We observe, during the 2 yr of hydroacoustic monitoring, that the transform faults on and bounding the plateau exhibit the highest seismic level and that ridge segments are not very active. Nevertheless, due to large location uncertainties, it is not always clear which events are related to either of these structures.

While seismicity and ridge segmentation are clearly related along the SEIR, the seismicity of the SWIR, particularly east of the Melville FZ, reflects large-scale lithospheric and asthenospheric behaviours. The level of seismicity decreases from the Gallieni FZ to the easternmost part of the SWIR, as the ridge deepens (Mendel *et al*. 1997; Cannat *et al*. 1999), and shear-wave velocities in the upper mantle (∼100 km; Debayle & Lévêque 1997) and mantle Bouguer anomalies (Cannat *et al*. 1999) increase, pointing to an eastward decrease in mantle temperatures and melt supply (Meyzen *et al*. 2003), while serpentinized peridotites are abundant on the seafloor. The Melville FZ appears as a major boundary in terms of offset, segmentation, bathymetry, seafloor structure, crustal thickness, magma supply, mantle temperature and seismicity rate and distribution. East of Melville, the earthquakes are sparse, of low magnitudes and scattered, except at robust and thick volcanic segments (61.5°E and 65.5°E), as also observed along the Gakkel Ridge (Schlindwein *et al*. 2015). West of Melville, the seismic activity is higher and large earthquakes ($M_w \geq 5$) are more abundant and focused along the ridge segments, suggesting segment-scale variations in a stronger and/or thicker brittle layer. This conjunction of observations suggests that the large-scale trend in the level of seismicity is related to changes in lithospheric thickness and/or rheology. At the considered level of completeness ($m_b > 3.3$), FZs appear to slip aseismically or through smaller magnitude earthquakes. Our 2 yr period of observation may also not be fully representative of the tectonic dynamics of ultraslow-spreading ridges.

### 5.3 Modes of seafloor accretion in the Indian Ocean

The two earthquake swarms recorded in 2012 on a spreading centre of the SEIR, at ∼29°S probably reflect magmatic events, which are the main processes leading to the creation of the upper oceanic crust. This conclusion is based on the distribution of events in time, the lack of an initial main shock and the uniform source level of the events, which differ from classical shock-aftershock sequences, and on the comparison with similar clusters observed in the Northeast Pacific (e.g. Dziak *et al*. 1995; Fox & Dziak 1998; Dziak & Fox 1999). Moreover, both swarms occur at the centre of a ridge-segment, where magmatic events are thought to focus (e.g. Cannat 1996; Fialko & Rubin 1998; Dziak & Fox 1999; Goslin *et al*. 2012; Grandin *et al*. 2012). The size and duration of cluster C1 are roughly similar to those observed on the Juan de Fuca (Dziak *et al*. 1995), although the relative small rate (0.05 m $s^{-1}$) and large onset time (30–40 hr) of the migration suggest that the magmatic episode did not lead to an eruption, following the migration rate and onset time criteria of Dziak *et al*. (2007). A migration of epicentres is generally interpreted as the result of a lateral injection of magma through the crust at shallow depth (e.g.

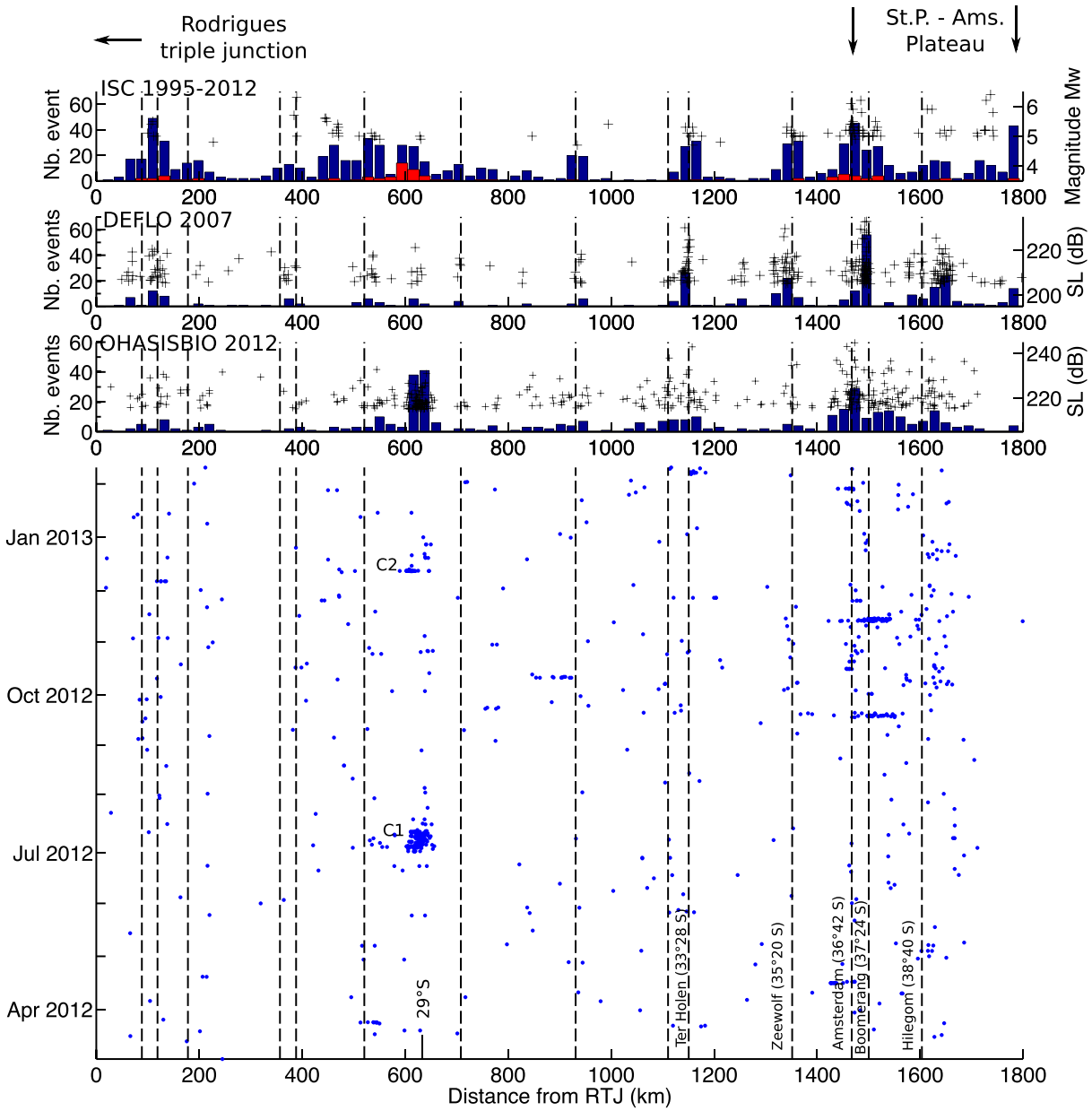


**Figure 9.** Spatial and temporal distribution of the seismicity along the Southeast Indian Ridge. In the ISC histogram, events in red (87 events) are those recorded in 2012. C1 and C2 are two clusters described in the text and illustrated in Figs 10 and 11. Same legend as Fig. 6.

Dziak *et al*. 1995; Dziak & Fox 1999; Bohnenstiehl *et al*. 2004). However, cluster C2, just few kilometres north of C1, does not display any migration pattern and lasted only few hours with fewer events (64). In size and duration the C2 swarm is more similar to the March 2001 swarm at Lucky Strike segment on the MAR, which was interpreted as a magma replenishment event (Dziak *et al*. 2004). Although the C1 and C2 episodes display a broad-band (5–30 Hz) energy, as found during the Lucky Strike episodes, no particular volcanic tremor is recognized afterwards that could evidence an eruptive event (e.g. Dziak & Fox 2002; Bohnenstiehl *et al*. 2014).

We therefore interpret the July and December 2012 swarms as episodes of dike or magma emplacement at shallow depth. Based on previously documented magmatic swarms, such events are often associated with an active volcanic structure and/or hydrothermal activity. The migration of the epicentres, indicating a lateral dike injection also suggests a shallow structure, probably 2–3 km deep, as deduced from similar events on the Juan de Fuca ridge or EPR. (Dziak & Fox 1999; Waldhauser & Tolstoy 2011). As observed on the Axial or Krafla volcanoes (e.g. Einarsson & Brandsdottir 1980; Dziak *et al*. 2012), a repeated volcano-tectonic activity may be precursory to an increased volcanic activity along this ridge segment that further hydroacoustic monitoring could confirm. Apart from these events, the SEIR segments are mostly aseismic during the 2 yr of observations (2007 and 2012), suggesting that seafloor spreading occurs through very episodic magma intrusions or with a seismic level below the level of completeness (i.e. detection threshold) of the AUH networks.

Along the SWIR, no such magmatic episode is observed in 2007 and 2012, although they are not uncommon for ultraslow-spreading ridges (Schlindwein 2012). Several magmatic swarms, large enough to be recorded by land-based stations, have been reported along the Gakkel Ridge (Tolstoy *et al*. 2001; Schlindwein *et al*. 2005) and in

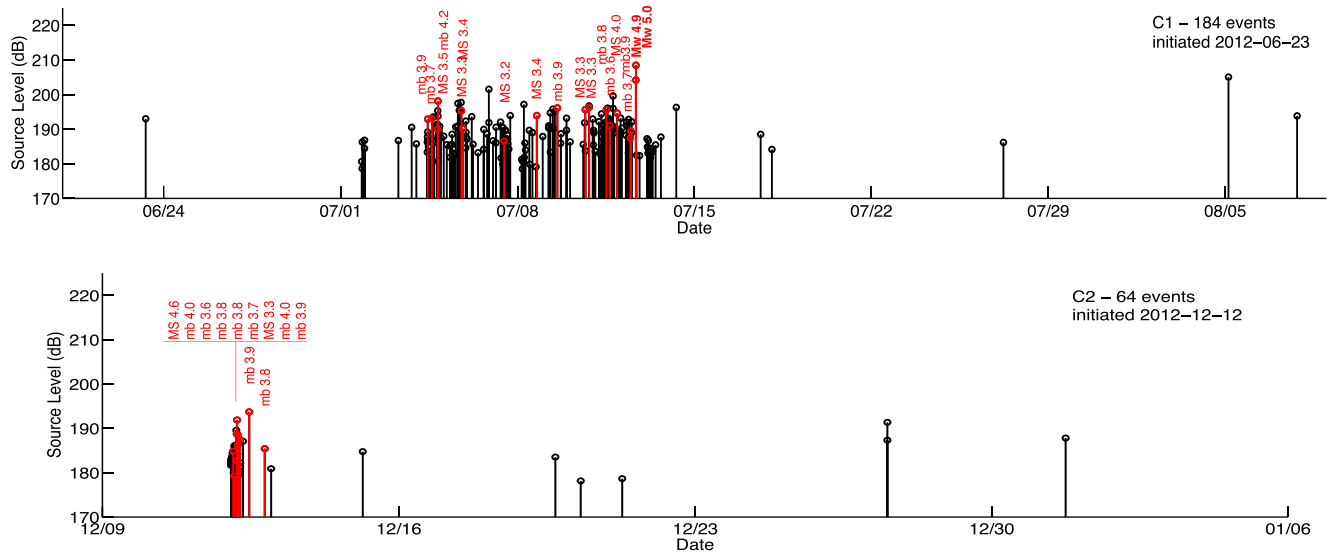


**Figure 10.** Time versus source level (magnitude) history of the two clusters observed in 2012 at 29°S along the Southeast Indian Ridge (C1, top and C2, bottom; Fig. 11). Events also recorded by land-based stations are shown in red. Both sequences lack a dominant main shock, which suggests a magmatic rather than a tectonic origin for these clusters.

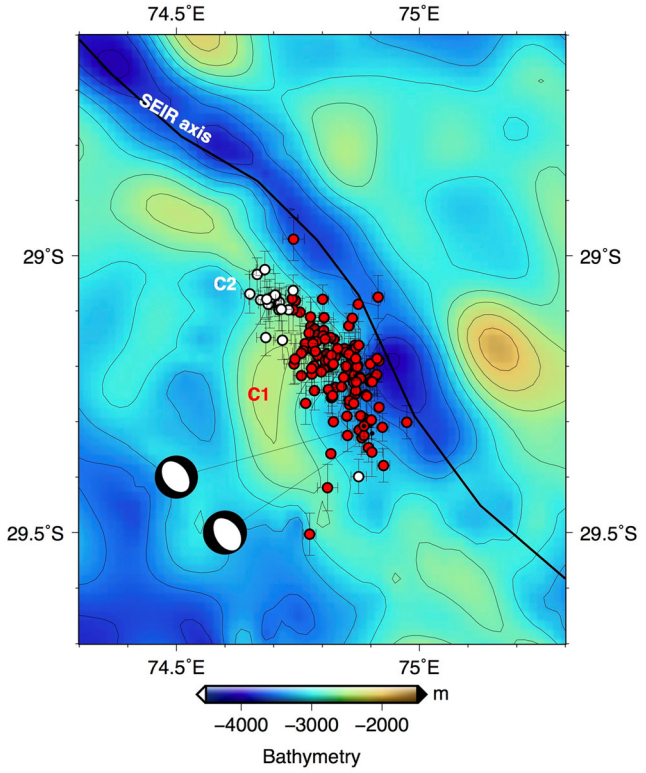


**Figure 11.** Location of the two clusters that occurred along the Southeast Indian Ridge in July 2012 (C1, red) and December 2012 (C2, white). Only events with location uncertainties <5 km are shown. The black line is the ridge axis inferred from the Smith & Sandwell (1997) satellite-derived 1′ bathymetry grid (background).

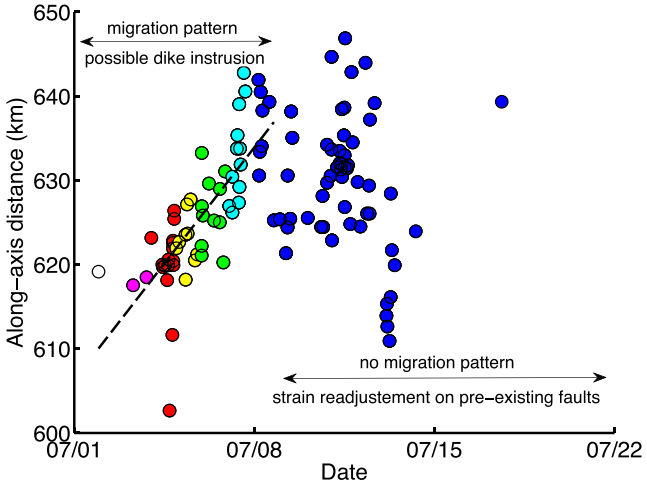


**Figure 12.** Time–distance distribution of cluster C1, in July 2012. Only events with location uncertainties <5 km are shown. A clear migration pattern is observed and epicentres continuously migrate to the south, along the axis, during almost 10 d, with 0.05 m $s^{-1}$ migration rate determined by linear regression. After 2012 July 8, events seem to occur along the whole segment section, suggesting a stress readjustment, as the dike no longer propagates. Colour changes up to 8 July enhance the daily progression.

the westernmost part of the SWIR (Läderach *et al*. 2012), generally associated with large volcanic edifices in the axial valley. Similar patterns of seismicity are observed along the SWIR and Gakkel Ridge, where robust magmatic segments produce large magnitude seismicity and swarms, unlike non-volcanic segments where the seismicity rate is low (Schlindwein *et al*. 2015). On the SWIR, where large areas of amagmatic seafloor are observed (Sauter *et al*. 2001; Cannat 1996), the oceanic extension is mainly accommodated by large detachment faults exhuming mantle-derived rocks (Sauter *et al*. 2013). The seismic behaviour of these faults is not fully understood, particularly in the presence of serpentinized peridotites, which could promote aseismic slips. The AUH seismicity thus reflects different kinds of tectonic processes, such as segment cooling, magma migration in the lithosphere or normal faulting in the rift valley rather than mantle exhumation processes. We note that earthquakes located in the amagmatic segment of the Gakkel Ridge have a higher frequency content than in the adjacent volcanic segments (Morozov *et al*. 2016). These observations outline a peculiar mechanical behaviour of amagmatic zones that a local OBS survey would help characterizing.

## 6 CONCLUSIONS

In 1 yr of hydroacoustic monitoring, about 1400 events have been recorded along 4000 km of two MORs in the Indian Ocean. The derived catalogue of seismicity contains nearly 10 times more events than the seismic land-based catalogues and has a completeness level of $m_b \geq 3.3$.

Although spreading rates between the SWIR and the SEIR are different, the overall averaged seismicity rates over both ridges are similar, showing that there is no systematic relationship between spreading and seismicity rates. Instead, the along-axis distribution of the seismic events seems more directly related to the accretion modes prevailing along each spreading system. Events are sparse and scattered but regularly distributed along the SWIR axis, especially from the RTJ to the Melville FZ. In addition, earthquakes are mainly located south of the median valley, along faults flanking the abyssal hills, parallel to the ridge axis. Whether they reflect an off-axis tectonic extension in an exposed serpentinized mantle or biases in the hydroacoustic approach is an interesting issue raised by this observation. The Melville FZ appears as a major boundary, separating two different seismic regimes and crustal accretion processes. Along the SEIR, on the contrary, events tend to cluster at ridge-segment ends and transform faults, while segments centres are almost aseismic or quiet, except for two large magmatic swarms at the centre of one segment. This seismicity distribution thus looks controlled by segment-scale crustal heterogeneities along the SEIR and by regional-scale contrasting accretion processes along the SWIR.

There is evidence for a repeated magmatic activity at a segment centre of the SEIR, while tectonic processes focus at segment ends. The observed swarms present characteristics of a magmatic emplacement at shallow depth, as observed on both intermediate and slow-spreading ridges. Both episodes suggest refilling of an active volcanic structure and might be precursors for an increase in the volcano-tectonic and hydrothermal activity. The imminent analysis of three complementary years of hydroacoustic records should address this question.

The general good agreement between hydroacoustic and teleseismic catalogues shows that in remote areas such as the Indian Ocean basins, the background seismicity observed in 1 yr by a hydroacoustic network is representative of the accumulated seismicity observed over two decades by land-based networks.

## ACKNOWLEDGEMENTS

The authors wish to thank the captains and crew of RV *Marion Dufresne* for the successful deployments and recoveries of the hydrophones of the OHASISBIO experiment. The French Polar Institute (IPEV) funded the ship-time for the deployment and recovery cruises (cruises VT110-MD189 and VT128-MD193). INSU-CNRS provided support for this acoustic experiment; the Regional Council of Brittany (CPER) funded the hydrophone moorings. We thank Andy Lau at PMEL for providing the Seas software. THS was supported by a fellowship from the University of Brest and from the Regional Council of Brittany, through *Laboratoire d'Excellence Labex MER* (grant ANR-10-LABX-19). Maps were made with the Generic Mapping Tool (GMT; Wessel *et al*. 2013) and Daniel Sauter kindly provided the SWIR bathymetric grids. This paper benefited from fruitful discussions with D.R. Bohnenstiehl and R.P. Dziak and insightful reviews from V. Schlindwein and J.-A. Olive.

## REFERENCES

Aki, K., 1965. Maximum likelihood estimate of $b$ in the formula $\log N = a - bM$ and its confidence limits, *Bull. Earthq. Res. Inst. Univ. Tokyo,* **43,** 237–239.

Beaulieu, S.E., 2010. 'InterRidge global database of active submarine hydrothermal vent fields, Version 2.0'. Available at: http://www.interridge.org/IRvents, last accessed 1 August 2014.

Bergman, E.A., Nabelek, J.L. & Solomon, S.C., 1984. An extensive region of off-ridge normal-faulting earthquakes in the Southern Indian Ocean, *J. geophys. Res.,* **89,** 2425–2443.

Bohnenstiehl, D.R. & Dziak, R.P., 2008. Mid-ocean ridge seismicity, in *Encyclopeda of Ocean Sciences*, eds Steele, J., Thorpe, S. & Turekian, K., Academic Press.

Bohnenstiehl, D.R., Tolstoy, M., Dziak, R.P., Fox, C.G. & Smith, G., 2002. Aftershock sequences in the mid-ocean ridge environment: an analysis using hydroacoustic data, *Tectonophysics,* **354,** 49–70.

Bohnenstiehl, D.R, Dziak, R.P, Tolstoy, M., Fox, C.G. & Fowler, M.J., 2004. Temporal and spatial history of the 1999–2000 Endeavour segment seismic series, Juan de Fuca ridge, *Geochem. Geophys. Geosyst.,* **5,** Q09003, doi:10.1029/2004GC000735.

Bohnenstiehl, D.W., Dziak, R.P., Matsumoto, H. & Conder, J.A., 2014. Acoustic response of submarine volcanoes in the Tofua Arc and northern Lau Basin to two great earthquakes, *Geophys. J. Int.,* **196,** 1657–1675.

Cannat, M., 1996. How thick is the magmatic crust at slow spreading oceanic ridges?, *J. geophys. Res.,* **101,** 2847–2857.

Cannat, M. *et al.*, 1995. Thin crust, ultramafic exposures and rugged faulting patterns at the Mid-Atlantic Ridge (22°–24°N), *Geology,* **23,** 49–52.

Cannat, M., Rommevaux-Jestin, C., Sauter, D. & Mendel, V., 1999. Formation of the axial relief at the very slow spreading Southwest Indian Ridge (49° to 69°E), *J. geophys. Res.,* **104,** 22 825–22 843.

Cannat, M., Sauter, D., Mendel, V., Ruellan, E., Okino, K., Escartin, J., Combier, V. & Baala, M., 2006. Modes of seafloor generation at a melt-poor ultraslow-spreading ridge, *Geology,* **34,** 605–608.

Cannat, M., Sauter, D., Bezos, A., Meyzen, C., Humler, E. & Le Rigoleur, M., 2008. Spreading rate, spreading obliquity, and melt supply at the ultraslow spreading Southwest Indian Ridge, *Geochem. Geophys. Geosyst.,* **9,** Q04002, doi:doi:10.1029/2007GC001676.

Chapp, E., Bohnenstiehl, D.R. & Tolstoy, M., 2005. Sound-channel observations of ice-generated tremor in the Indian Ocean, *Geochem. Geophys. Geosyst.,* **6,** Q06003, doi:10.1029/2004GC000889.

Debayle, E. & Lévêque, J.J, 1997. Upper mantle heterogeneities in the Indian Ocean from waveform inversion, *Geophys. Res. Lett.,* **24,** 245–248.

DeMets, C., Gordon, R.G. & Argus, D.F., 2010. Geologically current plate motions, *Geophys. J. Int.,* **181,** 1–80.

D'Eu, J.F., Royer, J.-Y. & Perrot, J., 2012. Long-term autonomous hydrophones for large-scale hydroacoustic monitoring of the oceans, in *OCEANS, 2012–Yeosu*, pp. 1–6, IEEE, doi:10.1109/OCEANS-Yeosu.2012.6263519.

Dick, H.J.B., Lin, J. & Schouten, H., 2003. An ultraslow-spreading class of ocean ridge, *Nature,* **426**(6965), 405–412.

Dziak, R.P. & Fox, C.G., 1999. The January 1998 Earthquake swarm at Axial Volcano, Juan de Fuca Ridge: hydroacoustic evidence of seafloor volcanic activity, *Geophys. Res. Lett.,* **26,** 3429–3432.

Dziak, R.P. & Fox, C.G., 2002. Evidence of harmonic tremor from a submarine volcano detected across the Pacific Ocean basin, *J. geophys. Res.,* **107,** ESE-1–ESE 1-11.

Dziak, R.P., Fox, C.G. & Schreiner, A.E., 1995. The June-July 1993 seismoacoustic event at CoAxial segment, Juan de Fuca Ridge: evidence for a lateral dike injection, *Geophys. Res. Lett.,* **22,** 135–138.

Dziak, R.P., Smith, D.K., Bohnenstiehl, D.R., Fox, C.G., Desbruyeres, D., Matsumoto, H., Tolstoy, M. & Fornari, D.J., 2004. Evidence of a recent magma dike intrusion at the slow spreading Lucky Strike segment, Mid-Atlantic Ridge, *J. geophys. Res.,* **109,** B12102, doi:10.1029/2004JB003141.

Dziak, R.P., Bohnenstiehl, D.R., Cowen, J., Baker, E., Rubin, K., Haxel, J. & Fowler, M.J., 2007. Rapid dike emplacement leads to eruptions and hydrothermal plume release during seafloor spreading events, *Geology,* **35,** 579–582.

Dziak, R.P., Hammond, S.R. & Fox, C.G., 2011. A 20-year hydroacoustic time series of seismic and volcanic events in the Northeast Pacific Ocean, *Oceanography,* **24,** 280–293.

Dziak, R.P., Haxel, J.H., Bohnenstiehl, D.R., Chadwick, W.W., Nooner, S.L., Fowler, M.J., Matsumoto, H. & Butterfield, D.A., 2012. Seismic precursors and magma ascent before the April 2011 eruption at Axial Seamount, *Nat. Geosci.,* **5,** 478–482.

Einarsson, P. & Brandsdottir, B., 1980. Seismological evidence for lateral magma intrusion during the July 1978 deflation of the Krafla volcano in NE-Iceland, *J. Geophys.,* **47,** 160–165.

Ekström, G., Nettles, M. & Dziewonski, A.M., 2012. The global CMT project 2004–2010: centroid-moment tensors for 13,017 earthquakes, *Phys. Earth planet. Inter.,* **200–201,** 1–9.

Escartin, J., Hirth, G. & Evans, B., 1997. Effects of serpentinization on the lithopsheric strength of normal faulting at slow-spreading ridges, *Earth planet. Sci. Lett.,* **151,** 181–190.

Escartin, J., Hirth, G. & Evans, B., 2001. Strength of slightly serpentinized peridotites: implications for the tectonics of oceanic lithosphere, *Geology,* **29,** 1023–1026.

Fialko, Y.A. & Rubin, A.M., 1998. Thermodynamics of lateral dike propagation: implications for crustal accretion at slow spreading mid-ocean ridges, *J. geophys. Res.,* **103,** 2501–2514.

Fox, C. & Squire, V.A., 1994. On the oblique reflexion and transmission of ocean waves at shore fast sea ice, *Philos. Trans. Royal Soc. London A: Math. Physical and Engin. Sci.,* **347,** 185–218.

Fox, C.G. & Dziak, R.P., 1998. Hydroacoustic detection of volcanic activity on the Gorda Ridge, February-March 1996, *Deep Sea Res. II,* **45,** 2513–2530.

Fox, C.G., Matsumoto, H. & Lau, A.T.K., 2001. Monitoring Pacific Ocean seismicity from an autonomous hydrophone array, *J. geophys. Res.,* **106,** 4183–4206.

Frohlich, C. & Davis, S.D., 1990. Single-link cluster analysis as a method to evaluate spatial and temporal properties of earthquake catalogues, *Geophys. J. Int.,* **100,** 19–32.

Goslin, J. *et al.*, 2012. Spatiotemporal distribution of the seismicity along the Mid-Atlantic Ridge north of the Azores from hydroacoustic data: insights into seismogenic processes in a ridge-hot spot context, *Geochem. Geophys. Geosyst.,* **13,** Q02010, doi:10.1029/2011GC003828.

Grandin, R., Socquet, A., Doubre, C., Jacques, E. & King, G.C.P., 2012. Elastic thickness control of lateral dyke intrusion at mid-ocean ridges, *Earth planet. Sci. Lett.,* **319,** 83–95.

Gutenberg, B. & Richter, D.F., 1944. Frequency of earthquakes in California, *Bull. seism. Soc. Am.,* **34,** 185–188.

Hanson, J.A. & Bowman, J.R., 2005. Indian Ocean ridge seismicity observed with a permanent hydroacoustic network, *Geophys. Res. Lett.,* **32,** L06301, doi: 10.1029/2004GL021931.

Hirth, G. & Guillot, S., 2013. Rheology and tectonic significance of serpentinite, *Elements,* **9,** 107–113.

International Seismological Centre (ISC), 2013. '*On-line Bulletin'*. Available at: http://www.isc.ac.uk (last accessed 1 August 2014).

Johnson, K.T.M, Graham, D.W., Rubin, K.H., Nicolaysen, K., Scheirer, D.S., Forsyth, D.W., Baker, E.T. & Douglas-Priebe, L.M., 2000. Boomerang Seamount: the active expression of the Amsterdam-St. Paul hotspot, Southeast Indian Ridge, *Earth planet. Sci. Lett.,* **183,** 245–259.

Katsumata, K. *et al.*, 2001. Microearthquake seismicity and focal mechanisms at the Rodriguez Triple Junction in the Indian Ocean using ocean bottom seismometers, *J. geophys. Res.,* **106,** 30 689–30 699.

Kuo, B.-Y. & Forsyth, D.W., 1988. Gravity anomalies of the ridge-transform system in the South Atlantic between 31 and 34.5 S: upwelling centers and variations in crustal thickness, *Mar. Geophys. Res.,* **10,** 205–232.

Läderach, C., Korger, E.I.M, Schlindwein, V., Müller, C. & Eskstaller, A., 2012. Characteristics of tectonomagmatic earthquake swarms at the Southwest Indian Ridge between 16°E and 25°E, *Geophys. J. Int.,* **190,** 429–441.

Maia, M. *et al.*, 2011. Building of the Amsterdam-Saint Paul plateau: a 10 Myr history of a ridge-hot spot interaction and variations in the strength of the hot spot source, *J. geophys. Res.,* **116,** B09104, doi:10.1029/2010JB007768.

Mendel, V., Sauter, D., Parson, L. & Vanney, J.-R., 1997. Segmentation and morphotectonic variations along a super slow-spreading center: the Southwest Indian Ridge (57°E–70°E), *Mar. Geophys. Res.,* **19,** 505–533.

Meyzen, C., Toplis, M.J., Humler, E., Ludden, J.N. & Mevel, C., 2003. A discontinuity in mantle composition beneath the southwest Indian ridge, *Nature,* **421,** 731–733.

Minshull, T.A. & White, R.S., 1996. Thin crust on the flanks of the slow-spreading Southwest Indian Ridge, *Geophys. J. Int.,* **125,** 139–148.

Minshull, T.A., Muller, M.R. & White, R.S., 2006. Crustal structure of the Southwest Indian Ridge at 66°E: seismic constraints, *Geophys. J. Int.,* **166,** 135–147.

Morgan, J.P. & Chen, Y.J., 1993. Dependence of ridge-axis morphology on magma supply and spreading rate, *Nature,* **364,** 706–708.

Morozov, A.N., Vaganova, N.V., Ivanova, E.V., Konechnaya, Y.V., Fedorenko, I.V. & Mikhaylova, Y.A., 2016. New data about small-magnitude earthquakes of the ultraslow-spreading Gakkel Ridge, Arctic Ocean, *J. Geodyn.,* **93,** 31–41.

Nyffenegger, P. & Frohlich, C., 2000. Aftershock occurrence rate decay properties for intermediate and deep earthquake sequences, *Geophys. Res. Lett.,* **27,** 1215–1218.

Reid, I. & Jackson, H.R., 1981. Oceanic spreading rate and crustal thickness, *Mar. Geophys. Res.,* **5,** 165–172.

Royer, J.-Y., Chateau, R., Dziak, R.P. & Bohnenstiehl, D.R., 2015. Seafloor seismicity, Antarctic ice-sounds, cetacean vocalizations and long-term ambient sound in the Indian Ocean basin, *Geophys. J. Int.,* **2,** 748–762.

Samaran, F., Stafford, K.M., Branch, T.A., Gedamke, J., Royer, J.-Y., Dziak, R.P. & Guinet, C., 2013. Seasonal and geographic variation of southern blue whale subspecies in the Indian Ocean, *PLoS One,* **8,** e71561.

Sauter, D., Whitechurch, H., Munschy, M. & Humler, E., 1991. Periodicity in the accretion process on the Southeast Indian Ridge at 27°40′S, *Tectonophysics,* **195,** 47–64.

Sauter, D., Patriat, P., Rommevaux-Jestin, C., Cannat, M. & Briais, A., 2001. The Southwest Indian Ridge between 49°15′E and 57°E: focused accretion and magma redistribution, *Earth Planet. Sci. Lett.,* **192,** 303–317.

Sauter, D., Carton, H., Mendel, V., Munschy, M., Rommevaux-Jestin, C., Schott, J.-J. & Whitechurch, H., 2004. Ridge segmentation and the magnetic structure of the Southwest Indian Ridge (at 50°30′E, 55°30′E and 66°20′E): implications for magmatic processes at ultraslow-spreading centers, *Geochem., Geophys., Geosyst.,* **5,** Q05K08, doi:10.1029/2003GC000581.

Sauter, D. *et al.*, 2013. Continuous exhumation of mantle-derived rocks at the Southwest Indian Ridge for 11 million years, *Nat. Geosci.,* **6,** 314–320.

Scheirer, D.S., Forsyth, D.W., Conder, J.A., Eberle, M.A., Hung, S.-H., Johnson, K. & Graham, D.W., 2000. Anomalous seafloor spreading of the Southeast Indian Ridge near the Amsterdam-St. Paul plateau, *J. geophys. Res.,* **105,** 8243–8262.

Schlindwein, V., 2012. Teleseismic earthquake swarms at ultraslow spreading ridges: indicator for dyke intrusions?, *Geophys. J. Int.,* **190,** 442–456.

Schlindwein, V., Müller, C. & Jokat, W., 2005. Seismoacoustic evidence for volcanic activity on the ultraslow-spreading Gakkel Ridge, Arctic Ocean, *Geophys. Res. Lett.,* **32,** L18306, doi:10.1029/2005GL023767.

Schlindwein, V., Demuth, A., Korger, E., Läderach, C. & Schmid, F., 2015. Seismicity of the Arctic mid-ocean ridge system, *Polar Sci.,* **9,** 146–157.

Simão, N., Escartín, J., Goslin, J., Haxel, J., Cannat, M. & Dziak, R.P., 2010. Regional seismicity of the Mid-Atlantic Ridge: observations from autonomous hydrophone arrays, *Geophys. J. Int.,* **183,** 1559–1578.

Small, C. & Sandwell, D.T., 1989. An abrupt change in ridge axis gravity with spreading rate, *J. geophys. Res.,* **94,** 17 383–17 391.

Smith, D.K., Tolstoy, M., Fox, C.G., Bohnenstiehl, D.R., Matsumoto, H. & Fowler, M.J., 2002. Hydroacoustic monitoring of seismicity at the slow-spreading Mid-Atlantic Ridge, *Geophys. Res. Lett.,* **29,** 13-1–13-4.

Smith, W.H.F. & Sandwell, D.T., 1997. Global sea floor topography from satellite altimetry and ship depth soundings, *Science,* **277,** 1956–1962.

Sykes, L.R., 1970. Seismicity of the Indian ocean and a possible nascent island arc between Ceylon and Australia, *J. geophys. Res.,* **75,** 5041–5055.

Tolstoy, M., Bohnenstiehl, D.R., Edwards, M.H. & Kurras, G.J., 2001. Seismic character of volcanic activity at the ultraslow-spreading Gakkel Ridge, *Geology,* **29,** 1139–1142.

Tucholke, B.E. & Lin, J., 1994. A geological model for the structure of ridge segments in slow spreading ocean crust, *J. geophys. Res.,* **99,** 11 937–11 958.

Waldhauser, F. & Tolstoy, M., 2011. Seismogenic structure and processes associated with magma inflation and hydrothermal circulation beneath the East Pacific, *Geochem. Geophys. Geosyst.,* **12,** Q08T10, doi:10.1029/2011GC003568.

Wessel, P., Smith, W.H., Scharroo, R., Luis, J. & Wobbe, F., 2013. Generic mapping tools: improved version released, *EOS, Trans. Am. geophys. Un.,* **94,** 409–410.

Yun, S., Ni, S., Park, M. & Lee, W.S., 2009. Southeast Indian Ocean-Ridge earthquake sequences from cross-correlation analysis of hydroacoustic data, *Geophys. J. Int.,* **179,** 401–407.